Automated Georeferencing and Extraction of Building Footprints from Remotely Sensed Imagery using Deep Learning

Aniruddha Khatua[a], Apratim Bhattacharya and Bharath H. Aithal[b]
Ranbir and Chitra Gupta School of Infrastructure Design and Management,
Indian Institute of Technology Kharagpur, Kharagpur, India

Keywords: Remote Sensing, GIS, Deep Learning, Automation, UAV Data Processing.

Abstract: Extracting building footprints from remotely sensed photos is crucial in conducting analyses in domains such as land-use analysis, transportation planning and development, environmental studies, and others. Various methodologies and strategies have been suggested for extracting building footprints from satellite or UAV images, aiming to circumvent the arduous, time-consuming, less effective, and costly process of manually digitizing building footprints. These proposed methodologies and strategies have demonstrated their efficacy in detecting and extracting features. However, they do not adequately retain the geographical information during the output generation process. This paper presents a pipeline that can automatically extract geographical information from input photos and transfer it to the output image, thereby achieving automated georeferencing of the output image. The pipeline utilizes the YOLOV8 model, an advanced deep-learning-based architecture for object detection and segmentation. The detection and segmentation findings, combined with the acquired geographical information, are used to perform vectorization and generate vector images of the extracted building footprint. This suggested pipeline streamlines the process of obtaining building footprint data linked to geospatial information by automating the georeferencing and shapefile preparation phases, reducing the associated complications. This automation not only expedites the process but also improves the precision and uniformity of the output datasets.

1 INTRODUCTION

The process of urbanization has experienced accelerated growth in the past twenty years because of globalization (Ramachandra et al., 2014). Urbanization, a significant driver of city expansion, is influenced by various elements, including economic, social, and political influences, as well as the geomorphology of urban regions. These growth factors stimulate investment, enhance the quality of public and private services, and foster technological innovation. Urban space refers to a human-dominated and altered environment that has been created through the process of urbanization (Bharath et al., 2018). The built-up density rises with population growth, modernization, and industrialization. Therefore, to ensure sustainable development, it is necessary to implement effective planning and meticulous design.

Buildings are acknowledged as one of the crucial components of urban areas. Identifying building types and extracting their footprints represent essential information within the realm of urban-related research. Obtaining the building information through GIS and integrating machine learning and remote sensing has significantly enhanced this process, resulting in improved accuracy and reduced time requirements. Annotated datasets have emerged as a vital prerequisite for developing and evaluating new automated techniques for interpreting remote sensing data. Unmanned Aerial Vehicle (UAV) imagery is an excellent means for training, annotating, testing, and automating the interpretation and data extraction procedures. The automated classification of building types and extracting their footprints from aerial imagery proved significant in deep learning, computer vision, and remote sensing (Goldberg et al., 2017; Ps & Aithal, 2022, Dey et al., 2024).

[a] https://orcid.org/0000-0002-4308-0595
[b] https://orcid.org/0000-0002-4323-6254

Khatua, A., Bhattacharya, A. and Aithal, B.
Automated Georeferencing and Extraction of Building Footprints from Remotely Sensed Imagery using Deep Learning.
DOI: 10.5220/0012625300003696

In *Proceedings of the 10th International Conference on Geographical Information Systems Theory, Applications and Management (GISTAM 2024)*, pages 128-135
ISBN: 978-989-758-694-1; ISSN: 2184-500X

Over the past few years, there has been a substantial surge in the application and advancement of deep learning methodologies across diverse domains. This trend is particularly pronounced in remote sensing, with a noteworthy increase in the integration and application of deep learning techniques. Many tasks, including feature extraction and classification, are now being conducted on various types of remotely sensed data, such as satellite and aerial images. Researchers have actively devised and implemented segmentation algorithms to enhance the efficiency and precision of surface feature extraction. Among the notable algorithms are modified versions of U-Net (Prakash et al., 2022; Madhumita et al., 2023), VGGNet (Simonyan & Zisserman, 2014), GoogleNet (Szegedy et al., 2015), ResNet (He et al., 2016), ImageNet (Krizhevsky et al., 2017), and Segnet (Badrinarayanan et al., 2017), among others. YOLOV8 (Jocher et al., 2023), an iteration of the You Look Only Once architecture (Redmon et al., 2016), has demonstrated promising outcomes in object detection and instance segmentation.

The investigation conducted by Khatua et al. (2023) delves into the noteworthy application of YOLOV8 within the geospatial domain, particularly in the classification of building rooftops. Their study involved categorizing building rooftops into two distinct classes, namely "Residential Buildings" and "Non-residential Buildings," which was achieved through the adept utilization of YOLOV8 for detection and segmentation. The researchers employed high-resolution datasets, specifically the open-source SpaceNet-3 Vegas dataset (satellite) and ISPRS Potsdam dataset (aerial), although the study area was outside India. Upon applying a similar methodology to an Indian dataset, an intriguing observation emerged: the model's output lacked geospatial information despite the input images being perfectly georeferenced. This necessitated an additional georeferencing step for the output images to make them suitable for subsequent geospatial analyses. In response to this challenge, this article proposes a refined approach to address the issue by introducing a systematic process for georeferencing the output images generated by the model.

Moreover, the article advocates for an automated procedure to extract building footprints in vector format enriched with geospatial information. This proposed enhancement ensures that the extracted building footprints maintain spatial references, significantly augmenting their utility and applicability for geospatial analyses. Including the georeferencing process is crucial for effortlessly incorporating the model's results into extensive geospatial workflows, thereby improving the overall efficiency of YOLOV8-based classification of building rooftops across various geographical settings.

2 METHODOLOGY

The methodology employed in this study adopts the building classification framework outlined by Khatua et al. (2023). The dataset used for this investigation is derived from an Indian source obtained through Aereo Manufacturing Private LTD., in conjunction with the SpaceNet-3 Vegas dataset. A meticulous annotation process was undertaken to categorize all images within the specified dataset into residential and non-residential classes. This annotated dataset was then utilized for training the YOLOV8 detection model—the initial phase of the training process involved exclusively using the SpaceNet-3 dataset. Once the model achieved satisfactory training accuracy on this dataset, the Indian dataset was introduced as an additional component to further enhance the model's robustness. After the successful training on both datasets, the model underwent testing using images deliberately held out from the training dataset. Upon completion of the result generation phase, the subsequent stage in the pipeline encompasses georeferencing and the production of vector images for the segmented and categorized buildings. This step involves translating the spatial information of the identified buildings and converting them into vector representations, contributing to a more comprehensive understanding of the built environment. Incorporating georeferencing and creating vector images guarantee both spatial precision and visual portrayal of the recognized building classifications, enhancing the overall efficiency of the classification procedure. Figure 1 depicts the entire methodology workflow.

In summary, the methodology unfolds systematically, starting with model training for classification, expanding to enhance the generalization capability, incorporating georeferencing to relate predictions to real-world locations, and generating vector polygons that capture the spatial distribution of segmented features. This stepwise approach ensures a robust and versatile pipeline-building analysis in diverse geographical contexts.

2.1 Dataset

This research utilized a diverse set of images, originating from various sources including aerial and satellite imaging. Satellite images are commonly available with embedded geospatial information and are often ortho-rectified, ensuring accurate geometric representation. Conversely, aerial images, while also typically accompanied by geospatial information, may lack orthorectification. In the specific context of this study, the dataset sourced from Aereo Manufacturing Private LTD., comprises aerial images that are not ortho-rectified; however, they are georeferenced.

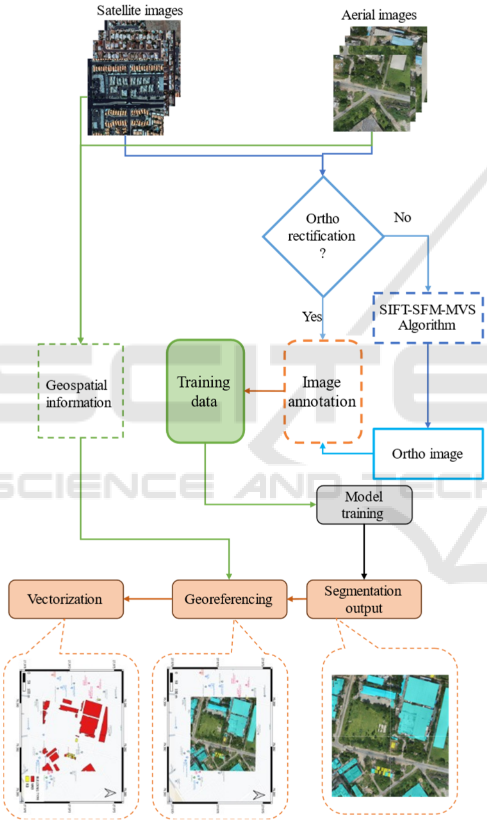

Figure 1: Methodology workflow.

2.1.1 SpaceNet-3 Dataset

The consortium of CosmiQ Works, Radiant Solutions, and NVIDIA has publicly released a significant satellite imagery collection annotated on the Amazon Web Services (AWS) platform under the name SpaceNet. SpaceNet partners have introduced public competitions to drive advancements in machine learning algorithms for remote sensing. This study utilized the SpaceNet 3 Las Vegas dataset (Figure 2), initially designed for road network extraction. Notably, the dataset includes diverse building images in size, shape, and architectural characteristics, proving advantageous for the model's comprehensive learning. The images are 1300x1300 pixels with a spatial resolution of 30cm.

2.1.2 Indian Dataset

The dataset (Figure 2) provided by Aereo Manufacturing Private LTD. includes images sized at 6000x4000 pixels, with a resolution of 3 centimetres. The bit depth of each image is 24, signifying the extent of color information encoded in each pixel. Furthermore, the images are structured in the RGB colour space.

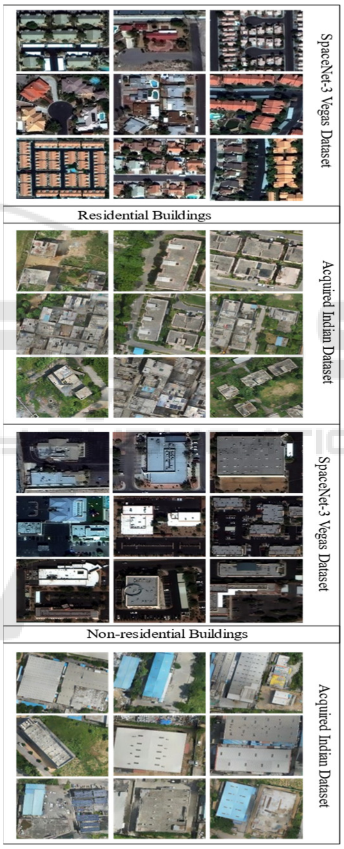

Figure 2: Example of residential and non-residential buildings.

2.2 Image Preprocessing and Ortho-Map Generation

Image preprocessing steps are implemented to generate orthorectified images (Figure 3) to enhance the quality and accuracy of the dataset. This crucial process corrects geometric distortions in the original aerial images, aligning them with the Earth's surface and facilitating precise spatial analysis. Integrating georeferencing and orthorectification in the preprocessing phase is essential for ensuring the reliability and consistency of the dataset, enabling more accurate interpretations and analyses in subsequent stages of the research. The initial step in this process involves the creation of an ortho-mosaic map layer through aerial triangulation. This step is crucial for producing an accurately geolocated ortho map. The ortho-mosaic is generated using the SIFT-SFM-MVS algorithm, distinguishing itself from traditional photogrammetry. The SFM-MVS workflow comprises three essential stages. First, it involves identifying and matching key points, such as Scale Invariant Feature Transform (SIFT) (Lindeberg, 2012). Second, the process entails performing Structure-from-Motion (SFM) (Schonberger & Frahm, 2016) with camera parameters to generate a sparse point cloud as output. Third, a densified point cloud is generated through the Multi-View-Stereo (MVS) process (Iglhaut et al., 2019). Firstly, the SIFT-SFM-MVS method offers automatic identification and matching of image features, even when they exhibit variations in scale, viewing angles, and orientations. This feature is mainly for small and unstable platforms. Secondly, the algorithm equations can be solved without necessitating information about the camera positions or ground control points, although these can be incorporated if available. Lastly, the approach allows for the automatic calibration or refinement of camera parameters during the processing. Following the generation of the ortho map, it is further organized into equal-sized grid-based tiles, each measuring 960x960, for efficient data management. The division enhances the overall organization and accessibility of the geospatial data.

2.3 Model Training and Output Generation

The study utilized YOLOV8 detection model as the detection component, sharing a design lineage with YOLOV5 (Jocher et al., 2020) through their common creator Ultratlytics. YOLOV8 introduces the C2f module, which combines two convolutional modules to improve detection by blending high-level and contextual features. It is an anchor-free model with a separate head for independently managing detection, classification, and regression, enhancing its accuracy and efficiency.

The process begins with amalgamating two distinct image datasets, followed by meticulous annotation for each image. These annotated datasets are then carefully partitioned, allocating 70% for training, 20% for validation, and 10% for testing. The significance of the validation set lies in its role as a metric for assessing the precision and recall of the model, offering insights into its performance. Augmented versions of each image are systematically generated to enhance the training accuracy. The applied augmentation techniques encompass vertical flips, horizontal flips, mirroring, and a 90^0 rotation. The validation images facilitate prediction comparisons at every iteration throughout the training phase, contributing to the model's refinement. Upon achieving a satisfactory level of training accuracy, the model is deployed to predict outcomes on the images within the designated test dataset. This comprehensive approach ensures a robust and well-optimized model capable of generalizing to new data.

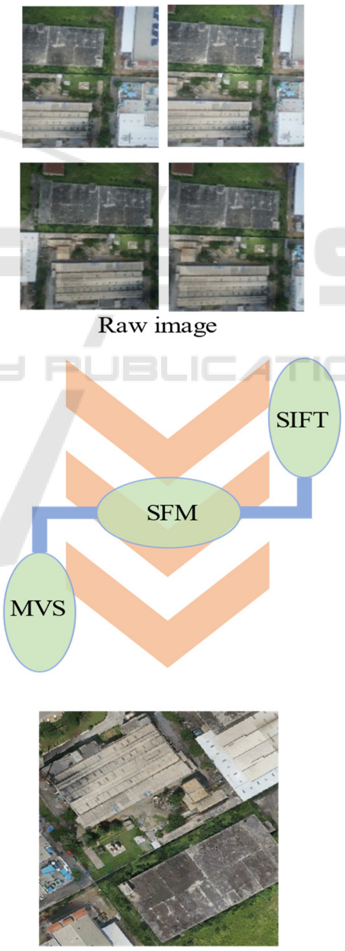

Raw image

Orthorectified image

Figure 3: Example of orthorectification.

2.4 Automated Georeferencing of the Model-Generated Outputs

The developed process demonstrates its effectiveness in generating a detailed mask that accurately outlines the recognized buildings. However, a significant drawback in the model's output becomes evident as it does not include crucial geospatial information. Acknowledging the vital role of geospatial information for extracting rooftop details, endeavours are focused on extracting this data. The needed geospatial details can be found in the original input images. The developed process demonstrates its effectiveness in generating a detailed mask that accurately outlines the recognized buildings. However, a significant drawback in the model's output becomes evident as it does not include crucial geospatial information. Acknowledging the vital role of geospatial information for extracting rooftop details, endeavours are focused on extracting this data. The needed geospatial details can be found in the original input images.

A systematic process is implemented to address this gap to extract georeferencing information from the input image. This process is executed with precision and efficacy by utilising an open-source Geospatial Data Abstract Library (GDAL) in the Python platform. The amalgamation of geospatial data is accomplished by employing the "georeference_image" function, as delineated in the following pseudo-code (Algorithm 1). This function serves as a crucial intermediary, transferring the extracted geospatial information from the input image to output generated by the YOLOV8 model. In essence, the strategic incorporation of georeferencing ensures that the model's outputs are visually accurate and possess spatial contexts needed for subsequent applications, such as vector image generation. Integrating the geospatial information to the output images elevates the overall utility of the pipeline, enabling more nuanced and context-aware analyses.

2.5 Vectorization of the Identified Objects

Once the segmented object coordinates transform into georeferenced coordinates, a crucial subsequent step involves connecting these newly acquired coordinates to create vector polygons. Figure 5 depicts the pseudo-code of the entire vectorization and polygon generation process. These polygons serve as geometric shapes on the map and play a vital role in representing the spatial distribution of the identified features. Importantly, these polygons encompass geographical coordinates and store additional information, such as the classification or type of the building, as attributes associated with each polygon. An essential detail lies in maintaining the consistency of the coordinate reference system (CRS) throughout the process. The coordinate reference system is a standardized way of representing location on the Earth's surface. In this case, the CRS used for the vector polygons is directly transferred from the original input image. This careful alignment ensures no error in the spatial positioning of the vector polygons. In other words, the geographic information encoded in the vector polygons precisely matches that of the initial image, eliminating any potential misalignment issues that could compromise the accuracy of subsequent analyses or applications.

```
Function
georeference_image(reference_tiff_path,
input_image_path,
output_georeferenced_path):

    Data: OPEN reference_tiff_path with gdal
    geo_transform: GET geo transformation
    from dataset;
    CALCULATE corner coordinates (Upper
    Left, Upper Right, Lower Left, and Lower
    Right);
    OPEN reference_tiff_path with rasterio as
    src_ref;
    GET reference image transform from src_ref
    OPEN input_image_path with rasterio as
    src_input
    READ input data and get input transform from
    src_input
    CREATE GroundControlPoints (GCPs) for
    input image corners
    CREATE transformation from GCPs
    UPDATE output_profile with transformation
    and CRS info
    OPEN output_georeferenced_path with
    rasterio for writing
    WRITE input_data with updated profile to
    output_georeferenced_path
end
```

Algorithm 1: Georeference Image.

3 RESULTS AND DISCUSSION

The methodology pipeline encompasses three key functionalities: building-type classification, georeferenced output generation, and vectorization of segmented features. The construction of this comprehensive pipeline unfolds in a stepwise manner to ensure its effectiveness. Initially, the YOLOV8 model undergoes training using the SpaceNet-3 dataset (Figure 4), focusing solely on validating the proper functioning of the classification process. This initial training phase is foundational, establishing the model's ability to accurately categorize building types.

```
    Function create_polygon_shapefile(output_shapefile_path, coordinates, reference_crs, names):

        DEFINE schema as dictionary with geometry and properties
        OPEN output_shapefile_path with fiona for writing with specified schema and reference CRS
        FOR EACH (coords, name) pair in ZIP(coordinates, names):
                CREATE polygon from coords
                WRITE polygon geometry and properties to output shapefile
                INCREMENT index
        RETURN output_shapefile_path
end
```

Algorithm 2: Creating vector polygons.

Following the successful validation, the pipeline expands by incorporating the preprocessed Indian dataset (Figure 5). The YOLOV8 model undergoes a subsequent round of training over this merged dataset to enhance its generalization capabilities. This iterative training approach, involving different datasets, ensures that the model can effectively handle diverse scenarios and accurately classify building types in varied geographical contexts.

Upon completion of the training process, the pipeline advances to the georeferencing stage. Here, geospatial information is seamlessly transferred to the output image, aligning it with real-world coordinates. This step is crucial for integrating the model's predictions with the broader geospatial context, enhancing the practical utility of the results. Finally, leveraging the geospatial information, the pipeline generates vector polygons. These polygons encapsulate the segmented features, providing a detailed spatial representation of the identified buildings. The vectorization process transforms pixel-based segmentations into geometric shapes, facilitating more nuanced and interpretable analyses. Figure 6 shows the entire output of the model pipeline.

The pipeline's detection and segmentation components utilize the YOLOV8 detection framework alongside the Segment Anything (SAM) model. Performance evaluation involves comparing this approach to other instance segmentation frameworks, including YOLOV8-seg and YOLOV5-seg. Notably, the YOLOV8-seg model outperforms its counterparts by achieving a higher mean average precision (mAP) at a 50% intersection over union (IoU) benchmark (Table 1). With 200 training epochs conducted on 800 images of 960x960 resolution, YOLOV8-seg notably completed training in the shortest time, clocking in at 0.45 hours. The integration of YOLOV8 for detection and SAM for segmentation has shown to be comparably effective to the standalone YOLOV8-seg model.

It's noteworthy that the implementation of this integrated technique entails a higher time investment compared to the alternative methods mentioned. In terms of detection efficiency, the study's showcased model outshines its counterparts by delivering quicker inference times. Specifically, the YOLOV8-seg model achieves an average processing time of around 400ms for a 960x960 image, encompassing pre-processing, inference, and post-processing phases. This contrasts with the YOLOV5's slightly longer processing time of 415 milliseconds, while the model proposed here marks a significant improvement with just 198 milliseconds needed (Table 1). In practical scenarios, such time differences might seem negligible for single-image analysis. However, this time efficiency becomes critically important when processing multiple images, highlighting the model's advantage in more demanding applications.

Table 1: Performance metrics values for different models.

Model	Precision	Recall	mAP	Avg. inference time (ms)
YOLOV8-seg	0.944	0.892	0.945	400
YOLOV5-seg	0.932	0.844	0.91	415
Proposed pipeline	0.929	0.838	0.899	198

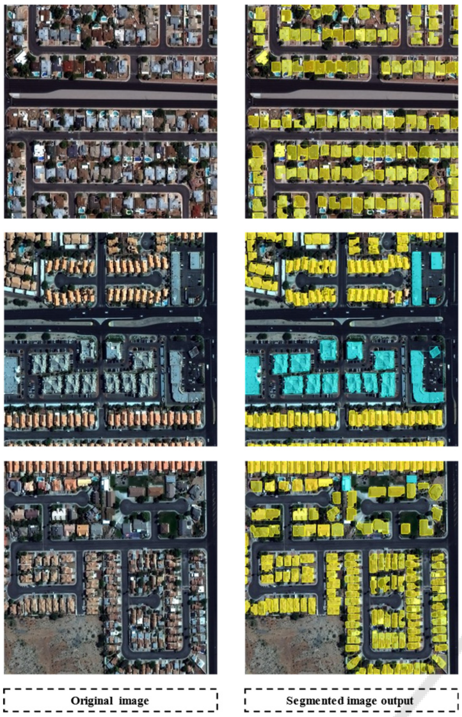

Figure 4: Examples of outputs of the pipeline for SpaceNet-3 dataset.

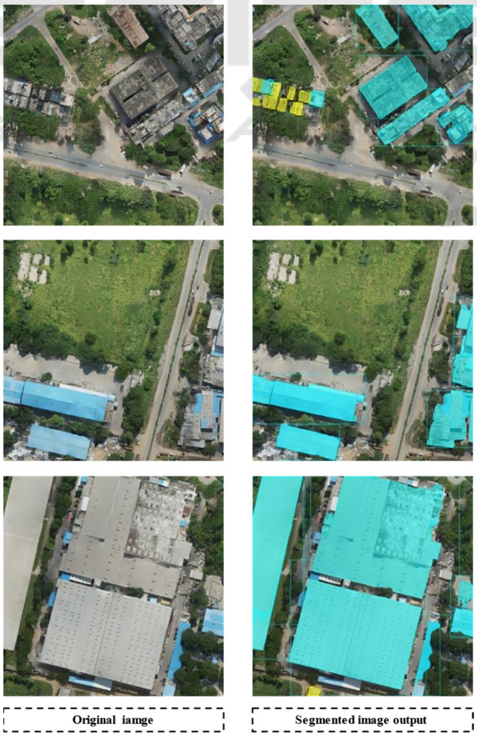

Figure 5: Examples of outputs of the pipeline for Indian dataset.

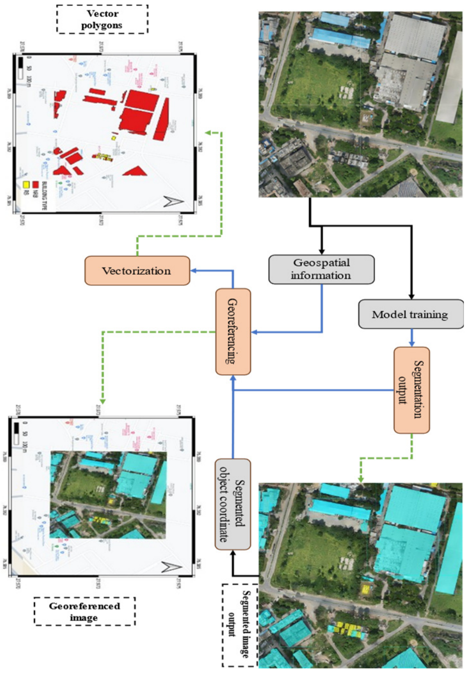

Figure 6: Example of entire pipeline outputs.

4 CONCLUSIONS

The research leveraged a pre-trained module that Khatua et al. (2023) introduced to extract distinctive building features from high-resolution remote-sensing images. Through comprehensive training and performance evaluation, the model produced output images or prediction maps that aligned with the input images' size, shape, coordinates, and datum. This consistent alignment facilitates subsequent spatial analyses, enhancing the interpretability of the results.

In the present scenario, it is noted that the YOLOV8-seg model outperforms other models in segmentation tasks. Yet, when considering inference speed, YOOV8+SAM leads the pack. The success of SAM in creating inferences is dependent on the detection capabilities of YOLOV8. This implies that SAM's ability to generate quick inferences is closely linked to how well YOLOV8 can detect objects.

The segmentation output from the pipeline conspicuously highlights the accurate extraction of most buildings, complete with relevant categorical information utilizing high-resolution remotely sensed images. This study effectively showcases the application of deep learning techniques to gain valuable insights into complex urban conditions. Furthermore, the demonstrated process is versatile, offering the potential for the application across various deep learning model outputs to extract geospatially relevant information.

ACKNOWLEDGEMENTS

We thank the Indian Institute of Technology Kharagpur Ranbir and Chitra Gupta School of Infrastructure Design and Management for financial and infrastructure support. We thank Aereo Manufacturing Private LTD. for providing us the aerial dataset on the Indian context.

REFERENCES

Badrinarayanan, V., Kendall, A., & Cipolla, R. (2017). Segnet: A deep convolutional encoder-decoder architecture for image segmentation. IEEE transactions on pattern analysis and machine intelligence, 39(12), 2481-2495.

Bayati, H., Najafi, A., Vahidi, J., & Gholamali Jalali, S. (2021). 3D reconstruction of uneven-aged forest in single tree scale using digital camera and SfM-MVS technique. Scandinavian Journal of Forest Research, 36(2–3), 210–220. https://doi.org/10.1080/02827581.2021.1903074

Bharath, H. A., Chandan, M. C., Vinay, S., & Ramachandra, T. V. (2018). Modelling urban dynamics in rapidly urbanising Indian cities. The Egyptian Journal of Remote Sensing and Space Science, 21(3), 201-210.

Dey, M., Prakash, P. S., & Aithal, B. H. (2024). UnetEdge: A transfer learning-based framework for road feature segmentation from high-resolution remote sensing images. Remote Sensing Applications: Society and Environment, 101160.

Goldberg, H., Brown, M., & Wang, S. (2017). A benchmark for building footprint classification using orthorectified RGB imagery and digital surface models from commercial satellites. *In 2017 IEEE Applied Imagery Pattern Recognition Workshop (AIPR)* (pp. 1-7). IEEE.

He, F., Liu, T., & Tao, D. (2020). Why resnet works? residuals generalize. IEEE transactions on neural networks and learning systems, 31(12), 5349-5362.

Iglhaut, J., Cabo, C., Puliti, S., Piermattei, L., O'Connor, J., & Rosette, J. (2019). Structure from motion photogrammetry in forestry: A review. *Current Forestry Reports,* 5(3), 155-168.

Jocher, G., Chaurasia, A., & Qiu, J. (2023). YOLO by Ultralytics (Version 8.0.0) *[Computer software].* https://github.com/ultralytics/ultralytics

Jocher, G., Nishimura, K., Mineeva, T., & Vilarino, R. (2020). Yolov5 by ultralytics. *Disponıvel em:* https://github. com/ultralytics/yolov5.

Khatua, A., Goswami, A. K., & Aithal, B. H. (2023). Deep learning-based automatic building types classification for transport planning. *Research for Transport and Logistics Industry (R4TLI), 8Th International Conference, Sri Lanka Society of Transport and Logistics*.

Krizhevsky, A., Sutskever, I., & Hinton, G. E. (2017). ImageNet classification with deep convolutional neural networks. Communications of the ACM, 60(6), 84-90.

Lindeberg, T. (2012). Scale Invariant Feature Transform. Scholarpedia, 7(5), 10491.

Ps, P., & Aithal, B. H. (2022). Building footprint extraction from very high-resolution satellite images using deep learning. *Journal of Spatial Science*, 1-17.

Ramachandra, T V &Aithal, Dr. Bharath & M V, Sowmyashree. (2014). Urban structure in Kolkata: metrics and modelling through geo-informatics. *Applied Geomatics*. 6. 1-16. 10.1007/s12518-014-0135-y.

Ramachandra, T. V., Aithal, B. H., & Sanna, D. D. (2012). Insights to urban dynamics through landscape spatial pattern analysis. International journal of applied earth observation and geoinformation, 18, 329-343.

Redmon, J., Divvala, S., Girshick, R., & Farhadi, A. (2016). You only look once: Unified, real-time object detection. In Proceedings of the IEEE conference on computer vision and pattern recognition (pp. 779-788).

Schonberger, J. L., & Frahm, J. M. (2016). Structure-from-motion revisited. *In Proceedings of the IEEE conference on computer vision and pattern recognition* (pp. 4104-4113).

Simonyan, K., & Zisserman, A. (2014). Very deep convolutional networks for large-scale image recognition. *arXiv preprint arXiv:1409.1556*.

Szegedy, C., Liu, W., Jia, Y., Sermanet, P., Reed, S., Anguelov, D., ... & Rabinovich, A. (2015). Going deeper with convolutions. In Proceedings of the IEEE conference on computer vision and pattern recognition (pp. 1-9).